

# Storage properties of a quantum perceptron

Aikaterini (Katerina) Gratsea,<sup>1</sup> Valentin Kasper,<sup>1</sup> and Maciej Lewenstein<sup>1,2</sup>

<sup>1</sup>*ICFO - Institut de Ciències Fotòniques, The Barcelona Institute of Science and Technology,  
Av. Carl Friedrich Gauss 3, 08860 Castelldefels (Barcelona), Spain*

<sup>2</sup>*ICREA, Pg. Lluís Companys 23, 08010 Barcelona, Spain*

(Dated: December 20, 2022)

Driven by growing computational power and algorithmic developments, machine learning methods have become valuable tools for analyzing vast amounts of data. Simultaneously, the fast technological progress of quantum information processing suggests employing quantum hardware for machine learning purposes. Recent works discuss different architectures of quantum perceptrons, but the abilities of such quantum devices remain debated. Here, we investigate the storage capacity of a particular quantum perceptron architecture by using statistical mechanics techniques and connect our analysis to the theory of classical spin glasses. Specifically, we focus on one concrete quantum perceptron model and explore its storage properties in the limit of a large number of inputs.

## I. INTRODUCTION

*Importance of machine learning.* The rapid development of machine learning algorithms revolutionized our day-to-day lives and created novel connections between such diverse fields as computer science and neuroscience [1], physics [2], and engineering [3]. At the core of the success of machine learning are deep artificial neural networks [4]. Whereas artificial neural networks initially had a biological motivation [5], the modern perspective considers artificial neural networks as a form of information processing [6–9].

*The quest for quantum advantage in quantum learning.* Machine learning algorithms have to be very efficient to handle a vast amount of information. This quest for efficiency created considerable interest to implement neural networks in dedicated hardware [10]. However, the usage of quantum hardware, especially quantum computers, motivates the question: How to use quantum mechanics best for machine learning purposes [11–16]? The quest for efficiency eventually led to the field of quantum machine learning, which now encompasses even more aspects [17], e.g., the application of machine learning techniques to analyze quantum systems and devices (cf. [2, 18–20]), but also the direct implementation of machine learning concepts on quantum hardware itself [13, 21]. In this work, we will be concerned with the latter perspective. One should fairly admit, however, that in the absence of large scale quantum computers with fault tolerant error correction, in the NISQ era [22], the question "Is quantum advantage the right goal for quantum machine learning?" is open [23, 24].

*Statistical mechanics of machine learning.* Statistical mechanics was introduced to study classical neural networks (NN) in the 1980s, mostly focusing on Hopfield-like attractor ANN [25, 26]. Then, Hopfield networks were studied as constraint satisfaction networks and also cognitive models, e.g. as a simple model for memory, but have never obtained any relevance for machine learning.

Their relationship with contemporary machine learning is typically considered to be remote. Restricted Boltzmann machines are related to them and do not fall out of fashion completely (cf. [27, 28] and references therein), but their working only partially relies on capacity estimates for Hopfield networks.

Recently, this situation starts to change with the progress of statistical methods that can be applied to classical feed-forward NNs and deep learning models [29]. Initially, feed forward NNs and deep learning (cf. [30, 31]) were considered very separately from ANNs, but nowadays statistical physics methods are being applied to feed forward NNs ([2, 29]. ANNs, and even the simple perceptrons, are back in the centre of interests with the advent of quantum technologies, due to the possible realization of simple quantum NNs with ultra-cold atoms, trapped ions, Rydberg atoms, super-conducting qubits, or photonic systems (cf. [32]). Importantly, tools of statistical physics have already established deep relations between neural networks, spin glasses, complexity, and information processing [14, 33]. One advantage of statistical physics is the computation of global properties of physical systems without knowing the microscopic details. Recently, there has been a true revival of increasing interest in using statistical physics techniques to study quantum information problems [2, 34].

One important application of statistical physics to information processing concerns the Hopfield-like networks or even simpler perceptrons. For example, there are many learning rules [35] for the Hopfield network, which can be used to obtain a desired input-output relations. Still, the connection between the global properties of the perceptron, and a specific learning rule might be challenging to analyze.

*Gardner's program.* In the seminal works [36, 37] Gardner addressed this challenge by using statistical physics to calculate the maximum storage capacity of a Hopfield network without referring to any specific learning rule. This approach of analyzing artificial networks without specifying the learning rule and treating the weights as a random variable is frequently referred to as Gardner's

program.

So far, the maximum storage capacity has also been considered for other QNN models [34, 38, 39]. In this work we apply Gardner's program to a specific quantum perceptron architecture proposed in [40], where the authors discuss a specific quantum analog of the classical perceptron - the building block of neural networks. This quantum perceptron model has a direct implementation on quantum hardware. We focus here on the maximal storage capacity of this proposal without referring to any learning rule.

*Gardner's program and quantum NNs.* The work of Gardner demonstrated that we can study Hopfield networks independent of the precise learning rule that is used. But, it is not only of considerable historical significance: it sheds light on the most important questions of contemporary quantum ML [23]. Moreover, it is extremely general, adaptive and versatile; so far it has been applied for very different models of quantum perceptrons or quantum neural networks, or even to calculate volumes of quantum correlated (entangled) states. Here is a list of selected examples and applications of Gardner's program for various models of quantum perceptrons, quantum NN and more:

- In ref. [41] quantum perceptron is defined as a unitary map followed by projective measurements in a multidimensional Hilbert space. Calculation of the relative volume reduces to calculation of the volume in the unitary group space.
- Gardner's relative volume approach clearly inspired the pioneering attempts to estimate volume of quantum correlated states, such as entangled states [42]. Integration consists in the first place in integration over unitary group in very high dimension, though.
- Recently, Gardner's program has been used on QNN models [43] corresponding to completely positive trace preserving maps (CPTP). Here relative volume requires integration over the space of maps.
- Gardner's program inspired investigation of the relative volume of parent Hamiltonians having a target ground state up to some fixed error  $\epsilon$  [44].
- A careful look on other models of quantum perceptrons immediately suggests that Gardner's approach is possible and might turn out to be useful as well. For instance, for the quantum perceptron models introduced in [45, 46] integration over the unitary group is needed to realize the Gardner's program.
- In the present paper, Gardner's program is applied to the specific quantum perceptron model proposed in [40].

By studying these models, we are one step closer to understand whether they provide a hope for quantum advantage.

*Plan of the paper.* This article is structured as follows: After motivating Gardner's program in this section, we discuss Gardner's program in detail and apply it to a quantum perceptron architecture in Sec. II. In Sec. III, we discuss the main result: the calculation of the storage capacity of a quantum perceptron by applying statistical physics techniques. Finally, we give the computational details of Gardner's program for the quantum perceptron in Sec. IV.

## II. QUANTUM PERCEPTRONS AND GARDNER'S PROGRAM

### A. Classical perceptron model

A classical perceptron is a function that maps a  $N$  dimensional input  $\vec{i}^\mu = (i_1^\mu, \dots, i_N^\mu)^T$  onto an output  $\sigma^\mu$ , where the weight vector  $\vec{w} = (w_1, \dots, w_N)^T$  determines the information processing. The additional label  $\mu \in \{1, 2, \dots, p\}$  denotes different pairs of input vectors and outputs [6, 33]. Moreover, we consider the following activation function

$$\sigma^\mu = \theta(\vec{i}^\mu \cdot \vec{w} - \kappa), \quad (1)$$

where  $\kappa$  is the threshold and  $\theta(\cdot)$  is the Heaviside function realizing the non-linearity of the perceptron model, see Fig. 1a.

### B. Quantum perceptron model

A quantum analog of the classical perceptron [40] is depicted in Fig. 1b with the corresponding quantum circuit in Fig. 1c. In this quantum perceptron the connection between the inputs, outputs and weights is given by the activation function

$$\sigma^\mu = \theta\left(\frac{1}{m}|\vec{i}^\mu \cdot \vec{w}|^2 - \kappa\right), \quad (2)$$

where the non-linearity of the perceptron is realized by the measurement, see Fig. 1b.

In the quantum case the input vector is  $\vec{i}^\mu = (i_0^\mu, \dots, i_{m-1}^\mu)^T$  and the weight vector is  $\vec{w} = (w_0, \dots, w_{m-1})^T$ , where  $m$  is the dimension of the Hilbert space. The vectors  $\vec{i}^\mu$  and  $\vec{w}$  are encoded in quantum states

$$|\psi_i\rangle = \frac{1}{\sqrt{m}} \sum_{j=0}^{m-1} i_j |j\rangle, \quad (3a)$$

$$|\phi_w\rangle = \frac{1}{\sqrt{m}} \sum_{j=0}^{m-1} w_j |j\rangle, \quad (3b)$$

respectively with the orthonormal basis vectors  $|j\rangle$  form the computational basis and we focused on the case of binary inputs and weights. The encoding unitary  $U_{\vec{i}}$  prepares the input state, while the processing unitary  $V_{\vec{w}}$  computes the inner product between  $\vec{i}$  and  $\vec{w}$ . The precise definition of the unitaries can be found in App. A. After the encoding and processing step (depicted by two blocks in Fig. 1c), a multi-controlled NOT gate is applied between the register and an ancilla qubit. Measuring the ancilla qubit in the computational basis gives  $|1\rangle$  with probability  $|\vec{i} \cdot \vec{w}|^2$ , see Fig. 1c and App. A for details.

### C. Gardner's program

The correct choice of the weights results in a desired input-output relation, i.e., a specific mapping between the input  $\vec{i}^\mu$  and the output  $\sigma^\mu$ . A learning rule is usually applied to find the correct weights, such as the Hebbian rule [38]. While the Hebbian rule has an appealing simplicity, Gardner, in her works [36, 37], was interested in the global properties of the classical perceptron model without specifying the learning rule. She asked the question: What is the maximum number of input-output patterns that the classical perceptron can realize? Therefore, she considered the relative volume in the space of possible weights, which realizes a given input-output relation.

### D. Storage capacity

Following Gardner's work, the storage capacity can be obtained from the fraction of  $\vec{w}$ -space which correctly reproduces the desired input-output relations normalized to the volume of vectors  $\vec{w}$ . When increasing the number of patterns, the volume of vectors  $\vec{w}$  typically shrinks, and the relative volume of the weights vanishes. The limit of vanishing relative volume defines the storage capacity of the perceptron [33]. From the definition of the storage capacity the difference between the classical and quantum perceptrons results from the different dimensionality of the input vectors, which equals  $N$  physical inputs for the classical perceptron. In contrast, in the quantum case, the number of inputs equals the dimension of the Hilbert space  $m$ . Hence, for the classical perceptron we have  $\alpha_c = p/N$ , while for the quantum perceptron  $\alpha_c = p/m$ . For the classical perceptron, the storage capacity is known to be 2 and was calculated for example in [14, 33, 36, 37].

### E. Calculation of the relative volume

In the following, we will focus on quantum perceptrons. The abundance of weights, which lead to desired

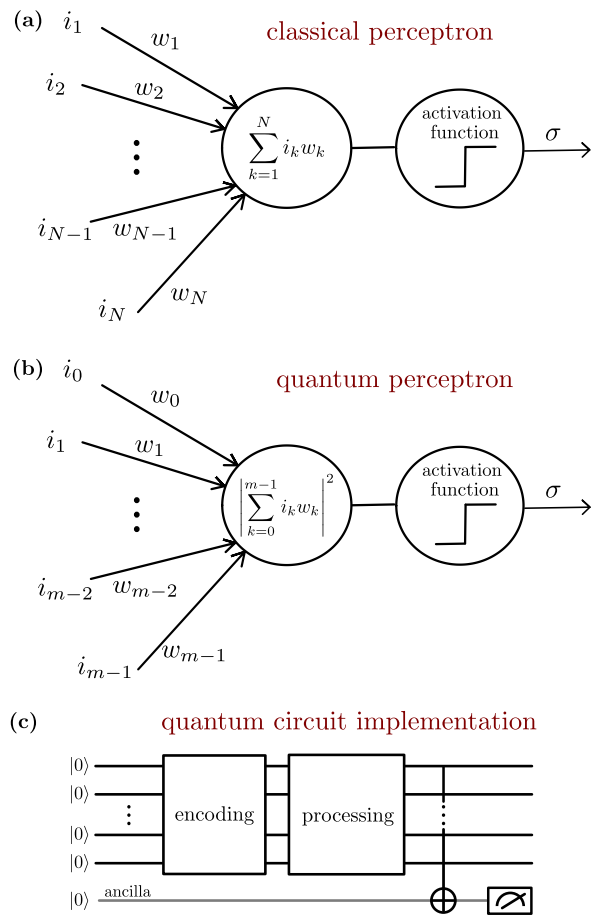


FIG. 1. **Classical and quantum perceptrons** (a) Schematic outline of the classical perceptron: An  $N$ -dimensional input array  $\vec{i}$  is processed with a weight vector  $\vec{w}$  such that  $\vec{i} \cdot \vec{w}$  enters the activation function. (b) Schematic outline of the quantum perceptron: An  $m$ -dimensional input array  $\vec{i}$  is processed with a weight vector  $\vec{w}$  to produce the inner product squared of these vectors. Both cases, the classical and the quantum, employ a non-linear activation leading to the output  $\sigma$ . (c) Quantum circuit implementation of the quantum perceptron following the work of Tacchino et al. [40]. An encoding unitary realizes the input state  $|\psi_{\vec{i}}\rangle$  and the processing unitary computes the inner product of the input and weight vectors. The outcome is then written on the ancilla qubit with a multi-controlled NOT gate. Finally, the activation is measured by the readout of the ancilla qubit.

input-output relations, can be treated by averaging over the weight vectors  $\vec{w}$ . This averaging gives rise to an ensemble of quantum machines, which can be analyzed with statistical physics tools. To define a finite volume of weights [37] we constrain the weight vector  $\vec{w}$ . Similar to Gardner's work one can consider two types of constraints: spherical weights, i.e.,  $|\vec{w}|^2 = m$  and Ising weights  $w_i = \pm 1$ . The corresponding integration mea-

asures [14] are

$$\rho_S[\vec{w}] = \frac{1}{V_{S_0}} \delta(|\vec{w}|^2 - m), \quad (4a)$$

$$\rho_I[\vec{w}] = \frac{1}{V_{I_0}} \prod_k [\delta(w_k - 1) + \delta(w_k + 1)] \quad (4b)$$

with the normalization (see Appendix B)

$$V_{S_0} = \int_w \delta(|\vec{w}|^2 - m), \quad (5a)$$

$$V_{I_0} = \int_w \prod_k [\delta(w_k - 1) + \delta(w_k + 1)]. \quad (5b)$$

Then the relative volume of perceptrons, which fulfill a specific input-output relation, is given by

$$V_M = \int_w \prod_\mu \theta\left(\frac{1}{m} |\vec{i}^\mu \cdot \vec{w}|^2 - \kappa\right) \rho_M[\vec{w}], \quad (6)$$

where the label  $M = S$  for the spherical constraint or  $M = I$  for the Ising constraint. The threshold  $\kappa$  takes values in  $[0, m]$  and in the limit  $\kappa \rightarrow 0$  the relative volume allows us to obtain the maximum storage capacity of the quantum perceptron model [14, 33]. We calculate the relative volume using the integral representation of the Heaviside function

$$\theta(y - \kappa) = \int_\kappa^\infty d\lambda \int_{-\infty}^\infty \frac{dx}{2\pi} e^{ix(\lambda - y)}, \quad (7)$$

which we insert into Eq. (6). In the following we outline the calculation of the relative volume for the case of spherical weights and present the details of the calculation in Sec. IV.

### 1. Spherical weights

The distribution of the spherical weights is given in Eq. (4a) and contains a delta function, which we represent via

$$\delta(|\vec{w}|^2 - m) = \int_{-\infty}^\infty \frac{dE}{2\pi} e^{iE(|\vec{w}|^2 - m)}. \quad (8)$$

Further, we average over the input vector  $\vec{i}^\mu$  to avoid bias towards specific input vectors. The average with respect to  $\vec{i}^\mu$  is denoted as  $\langle\langle \cdot \rangle\rangle$ . The expression for the relative volume becomes

$$\begin{aligned} \langle\langle V_S \rangle\rangle &= \frac{1}{V_{S_0}} \int_w \int_\lambda \int_x \int_E \exp[iE(|\vec{w}|^2 - m)] \\ &\times \langle\langle \exp\left[i \sum_\mu x^\mu \left(\lambda^\mu - \frac{1}{m} |\vec{i}^\mu \cdot \vec{w}|^2\right)\right] \rangle\rangle, \end{aligned} \quad (9)$$

where the integration measure is given in App. B.

Similar to Gardner we make the observation that Eq. (9) is a partition function of a classical spin glass, where  $\langle\langle \cdot \rangle\rangle$  is interpreted as a disorder average and  $\vec{w}$  is a classical spin variable. As for classical spin glasses [14, 33] we calculate  $\langle\langle \log V_S \rangle\rangle$  via the replica trick

$$\langle\langle \log V_S \rangle\rangle = \lim_{n \rightarrow 0} \frac{\langle\langle V_S^n \rangle\rangle - 1}{n}, \quad (10)$$

which leads to the replicated variables  $\vec{w}^\alpha$ ,  $x^\alpha$ ,  $\lambda^\alpha$  with the replica index  $\alpha \in \{1, \dots, n\}$ . In addition, we introduce the spin glass order parameter  $q^{\alpha\beta}$  and its conjugate  $F^{\alpha\beta}$  via the integral

$$\begin{aligned} 1 &= \int_{-\infty}^\infty dq^{\alpha\beta} \delta\left(q^{\alpha\beta} - \frac{1}{m} \sum_k w_k^\alpha w_k^\beta\right) \\ &= m \int_{-\infty}^\infty dq^{\alpha\beta} \int_{-\infty}^\infty \frac{dF^{\alpha\beta}}{2\pi} e^{imF^{\alpha\beta}\left(q^{\alpha\beta} - \frac{1}{m} \sum_k w_k^\alpha w_k^\beta\right)} \end{aligned} \quad (11)$$

with  $\alpha < \beta$ . This identity is also referred to as Hubbard-Stratonovich transformation, see [47, 48] for details.

### 2. Ising inputs

In the next step, we perform the average over the inputs and assume small fluctuations of  $x^\alpha$ , which leads to

$$\langle\langle V_S^n \rangle\rangle = \frac{1}{V_{S_0}^n} \int_F \int_q \int_E e^{mG}, \quad (12)$$

with integration measure given in App. B and where we introduced the effective potential

$$G = \alpha G_1[q^{\alpha\beta}] + G_2[E^\alpha, F^{\alpha\beta}] - i \sum_\alpha E^\alpha + i \sum_{\alpha < \beta} F^{\alpha\beta} q^{\alpha\beta} \quad (13)$$

with the storage capacity  $\alpha$  and the two contributions

$$\begin{aligned} G_1[q^{\alpha\beta}] &= \log \int_{-\infty}^\infty \prod_\alpha \frac{dx^\alpha}{2\pi} \int_\kappa \prod_\alpha d\lambda^\alpha \\ &\times \exp\left(i \sum_\alpha x^\alpha \lambda^\alpha - \frac{1}{2} \sum_\alpha (x^\alpha)^2 - \sum_{\alpha < \beta} (q^{\alpha\beta})^2 x^\alpha x^\beta\right) \end{aligned} \quad (14)$$

and

$$\begin{aligned} G_2[E^\alpha, F^{\alpha\beta}] &= \log \int_{-\infty}^\infty \prod_\alpha dw^\alpha \\ &\times \exp\left(i \sum_\alpha E^\alpha (w^\alpha)^2 - i \sum_{\alpha < \beta} F^{\alpha\beta} w^\alpha w^\beta\right). \end{aligned} \quad (15)$$

Comparing the integrals for the effective potential reveals a quadratic dependency on  $q^{\alpha\beta}$  for the quantum model

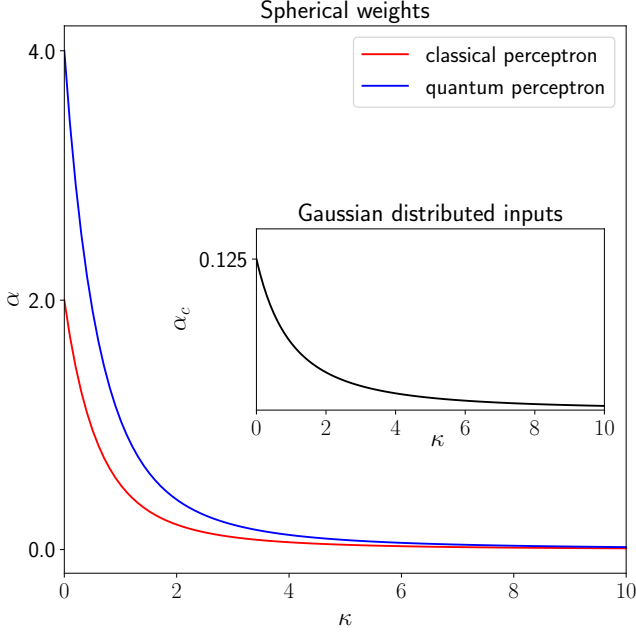


FIG. 2. **Storage properties of perceptrons for spherical weights:** Storage capacity for the classical (red) and quantum (blue) perceptrons as a function of the threshold  $\kappa$ . For  $\kappa \approx 0$ , the storage capacity has a maximum, whereas the storage capacity decays for  $\kappa \gg 1$ . In the inset, we plot the critical storage capacity as a function of  $\kappa$  for Gaussian distributed inputs.

and a linear dependence on  $q^{\alpha\beta}$  for the classical model within the exponents. The non-linear dependence in the quantum case is a consequence of the measuring process, which involves the modulus square.

After the Hubbard-Stratonovich transformation we perform a saddle-point approximation for large  $m$  and assume replica symmetry, i.e.,

$$q^{\alpha\beta} = q, F^{\alpha\beta} = F, E^\alpha = E. \quad (16)$$

The saddle-point equations are

$$\frac{\partial G}{\partial E} = \frac{\partial G}{\partial F} = \frac{\partial G}{\partial q} = 0, \quad (17)$$

which we solve and subsequently perform the limit  $n \rightarrow 0$ . Taking the derivative of  $G$  with respect to  $q$  and analyzing the limits  $q \rightarrow 1$  and  $\kappa \rightarrow 0$  leads to the maximum critical storage capacity of

$$\alpha_{c,\max} = 4. \quad (18)$$

Additionally, the saddle-point approximation allows us to study the critical storage capacity  $\alpha_c$  as a function of the threshold  $\kappa$ , which we depict in Fig. 2.

### 3. Gaussian distributed inputs

In this section, we discuss the case of inputs distributed according to a Gaussian normal distribution. The weights in turn are distributed according to Eq. (4a). We apply the replica trick Eq. (10), introduce the order parameters as in Eq. (11) and average over the inputs to calculate the effective potential  $G$ . A comparison to Eq. (12) reveals that only the expression for  $G_1$  changes

$$G_1[q^{\alpha\beta}] = \log \int_{-\infty}^{\infty} \prod_{\alpha} \frac{dx^{\alpha}}{2\pi} \int_{\kappa}^{\infty} \prod_{\alpha} d\lambda^{\alpha} \times \exp \left[ i \sum_{\alpha} x^{\alpha} \lambda^{\alpha} - \log \det \left( 1 + 2i\hat{A} \right) \right], \quad (19)$$

where we introduce the matrix  $A$  later in Eq. (46). Next, we assume replica symmetry, i.e.,

$$q^{ab} = q, F^{ab} = iF, \quad (20)$$

and the saddle-point equations are

$$\frac{\partial G}{\partial F} = \frac{\partial G}{\partial q} = 0, \quad (21)$$

which we solve and subsequently perform the limit  $n \rightarrow 0$ . The saddle-point equation given by the derivative with respect to  $q$  leads to

$$\alpha(2 + \kappa)^2 q = \frac{q}{2(1 - q)^2}. \quad (22)$$

This equation has one trivial solution  $q = 0$  and one non-trivial in  $0 < q < 1$ . The non-trivial solution exists if and only if

$$2\alpha(2 + \kappa)^2 \geq 1. \quad (23)$$

For  $\alpha \leq \alpha_c = (1/2)(2 + \kappa)^2$  the solution is trivial, and the logarithm of the relative volume is close to one, it is proportional to  $\alpha\kappa/2$ , and for  $\kappa = 0$  all perceptrons are activated. Above  $\alpha_c$ , the solution is non-zero, and the volume shrinks faster than exponentially with  $m$ . We plot  $\alpha_c$  in Fig. 2 for different values of  $\kappa$  and observe  $\alpha_c \rightarrow 1/8$  for  $\kappa = 0$ . The phase transition has different character in comparison to Gardner's work [36]. In her work, the volume decreases exponentially with  $m$  below the critical  $\alpha_c$  (where  $q < 1$ ), and strictly shrinks to zero above the critical  $\alpha_c$  (where  $q = 1$ ). In our work, the volume is close to one below  $\alpha_c$ , and it starts to shrink exponentially with  $m$  above.

### 4. Ising weights

In the classical case the Ising weights were treated for example in [14, 33, 37]. Here, we use the Ising weights for the quantum case and employ Eq. (4b) and Eq. (5)



for the integration measure and normalization of the volume, respectively. We apply the replica trick Eq. (10), introduce the order parameters Eq. (11) and average over the inputs to calculate the effective potential. The contribution  $G_1$  is the same as Eq. (15), while  $G_2$  becomes

$$G_2[F^{\alpha\beta}] = \log \sum_{\{w^\alpha = \pm 1\}} \exp \left( \sum_{\alpha < \beta} F^{\alpha\beta} w^\alpha w^\beta \right). \quad (24)$$

We assume replica symmetry, i.e.,

$$q^{ab} = q, F^{ab} = iF, \quad (25)$$

and the saddle-point equations are

$$\frac{\partial G}{\partial F} = \frac{\partial G}{\partial q} = 0. \quad (26)$$

Solving the saddle point equations in the limit for  $q \rightarrow 1$  we conclude that the storage capacity is

$$\alpha_c(\kappa) = \frac{4}{\pi} \left[ \int_{-\kappa}^{\infty} Dy (\kappa + y)^2 \right]^{-1}, \quad (27)$$

where we used the abbreviation

$$\int_{-\infty}^{\infty} Dy = \sqrt{\frac{1}{2\pi}} \int_{-\infty}^{\infty} dy e^{-\frac{y^2}{2}}. \quad (28)$$

In addition, we present the results of a Monte Carlo simulation in Fig. 3, which shows that as  $m \rightarrow \infty$ , the storage capacity approximately behaves as  $\alpha \rightarrow 0$  (see App. C for details). We interpret this discrepancy as the necessity for replica symmetry breaking. This analysis, however, goes beyond the scope of this paper.

### III. DISCUSSION

In this work, we calculate the storage capacity of a quantum perceptron, which was proposed in a recent work [40]. Following the seminal works of Gardner [36, 37], we use statistical physics techniques to calculate the storage capacity of this perceptron. In particular, we interpret this quantum perceptron as a classical perceptron on an extended input space with a different activation function, see Fig. 1. This interpretation allows us to calculate the storage capacity of a quantum perceptron by computing the relative volume of quantum perceptrons which fulfill a given input-output relation.

To handle the multitude of inputs and learning rules, we integrate over the input and the weights. Formally, this averaging over input and weights maps the calculation of the relative volume to the partition function of a classical spin glass problem. Similar to problems in classical spin glass theory, we compute the logarithm of the partition function using the replica trick [14, 33]. Further, by using the large  $m$  expansion, we can determine the storage capacity  $\alpha_c$  in leading order, which is the

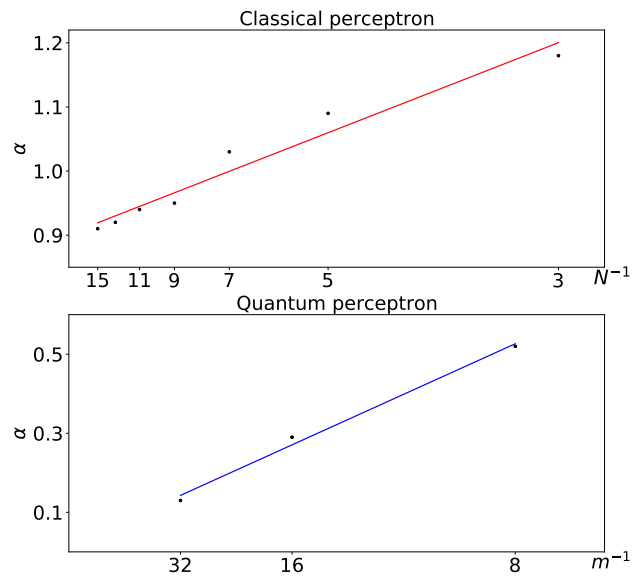


FIG. 3. **Storage properties of perceptrons for the Ising weights** Storage capacity for the classical (red) and quantum (blue) Ising perceptrons as a function of the number of inputs  $N^{-1}$  and  $m^{-1}$ , respectively. The dots are the result of the Monte Carlo simulations. The intersection of the lines with the  $y$ -axis gives the storage capacity  $0.86 \pm 0.01$  for the classical and  $0.010 \pm 0.005$  for the quantum perceptron in the limits  $N, m \rightarrow \infty$ .

ratio of the stored patterns  $p$  over the computational resources  $m$ . Notably, the techniques presented here are applicable to other quantum architectures.

Given the model of Fig. 1c, we obtain a maximal critical storage capacity of  $\alpha_{c,\max} = 4$  for the spherical weights, see Fig. 2. To put these results in perspective, we compare them with the classical perceptron. In the classical case, the maximal storage capacity is  $\alpha_{c,\max} = 2$ , see Fig. 2. With our definition of the storage capacity, the classical and quantum perceptron lead to the same order of magnitude when  $\kappa$  goes to zero. However, we emphasize that the input vector of the perceptron is determined by the number of inputs  $N$  in the classical case, but equals the dimension of the Hilbert space  $m$  in the quantum case. In particular, the number of classical inputs and the dimension of Hilbert space are connected via  $m = 2^N$ . Our results on the storage capacity are also in accordance with recent works [43, 49–51].

For Gaussian distributed inputs, the performance of the quantum perceptron is quite different from the classical perceptron in accordance with a related work [52]. In the classical case, the relative volume shrinks exponentially with  $m$  below the critical capacity, and shrinks suddenly to zero above  $\alpha_c$ , see [53]. In the present study, the volume shrinks exponentially with  $m$ , but the rate of shrinking changes from below ("easy learning" phase) to above  $\alpha_c$  ("hard learning" phase). The maximum storage capacity of the "easy learning" phase is 0.125.

For a classical perceptron with Ising weights, analyti-

cal calculations suggest that  $\alpha_{\max} = 0.83$  [54], while our Monte Carlo simulations gives  $\alpha_{\max} = 0.86 \pm 0.01$  [55]. In contrast to the classical case, the relative volume of interactions goes approximately to zero for quantum perceptrons with Ising weights according to our MC simulations. This is in accordance with results from the related work in [40], where they explore the learning capability of quantum perceptrons with Ising weights. They show that for each pattern stored a different set of weights is required. This result already suggests that it is hard to choose a weight that can store many patterns.

For future work, it would be highly important for practical applications to explore the storage properties of the quantum perceptron with correlated inputs or input-output patterns. In a previous analysis of quantum perceptrons [41], one distinguished between three different phases an *ignorant phase*, a *random phase*, and *learning phase*, and it would be interesting to detect these phases in the quantum perceptron architecture of [40]. Future studies should also investigate the storage capacity away from  $q \approx 1$  and the dependency on  $\kappa$ . Also, it will be essential to include corrections to the large  $m$  expansion and study the stability of the replica symmetric saddle point solution [48]. Finally, an exciting continuation of this work would be to consider other architectures of quantum perceptrons [45, 56, 57], e.g., qudit based platforms [58–60] and analyze them with the tools presented in this work.

#### IV. METHODS

In this section, we elaborate on the computational details presented in Sec. II, i.e., the averaging over the inputs, the calculation of the effective potential, and the saddle-point approximation.

##### A. Averaging over the input patterns

We perform the average  $\langle\langle\cdot\rangle\rangle$  and assume weak correlations between the weights. Then we can approximate

$$\langle\langle\prod_{\alpha,\mu} e^{-\frac{i}{m}x_\mu^\alpha|\vec{w}^\mu\cdot\vec{w}^\alpha|^2}\rangle\rangle \approx \prod_{\mu,k,l} \cos\left(\frac{1}{m}\sum_{\alpha}x_\mu^\alpha w_k^\alpha w_l^\alpha\right), \quad (29)$$

see [61] for details. Using Eq. (29) the relative volume becomes

$$\begin{aligned} \langle\langle V_S \rangle\rangle &= \frac{1}{V_{S_0}^n} \int_w \int_\lambda \int_x \int_E \int_q \int_F \\ &\times \exp\left[i\sum_{\alpha,\mu}x_\mu^\alpha\lambda_\mu^\alpha + \sum_{\mu,k,l}\log\cos\left(\frac{1}{m}\sum_{\alpha}x_\mu^\alpha w_k^\alpha w_l^\alpha\right)\right] \\ &\times \exp\left[iE^\alpha(|\vec{w}^\alpha|^2 - m) + imF^{\alpha\beta}(q^{\alpha\beta} - \frac{1}{m}\sum_k w_k^\alpha w_k^\beta)\right]. \end{aligned} \quad (30)$$

Next, we use the approximation  $\log\cos x \approx -x^2/2$  and use Eq. (11). In addition, we employ that the integral

$$\begin{aligned} I &= \int_{-\infty}^{\infty} \prod_{\alpha,\mu} \frac{dx_\mu^\alpha}{2\pi} \int_{\kappa}^{\infty} \prod_{\alpha,\mu} d\lambda_\mu^\alpha \\ &\times \exp\left(i\sum_{\alpha,\mu}x_\mu^\alpha\lambda_\mu^\alpha - \frac{1}{2}\sum_{\mu,\alpha}(x_\mu^\alpha)^2 - \sum_{\alpha<\beta,\mu}(q^{\alpha\beta})^2 x_\mu^\alpha x_\mu^\beta\right) \end{aligned} \quad (31)$$

factorizes according to

$$\begin{aligned} I &= \left[ \int_{-\infty}^{\infty} \prod_{\alpha} \frac{dx^\alpha}{2\pi} \int_{\kappa}^{\infty} \prod_{\alpha} d\lambda^\alpha \right. \\ &\times \left. e^{i\sum_{\alpha}x^\alpha\lambda^\alpha - \frac{1}{2}\sum_{\alpha}(x^\alpha)^2 - \sum_{\alpha<\beta}(q^{\alpha\beta})^2 x^\alpha x^\beta} \right]^p, \end{aligned} \quad (32)$$

which leads to Eq. (12) - (15).

##### B. Calculation of $G_1$

We assume replica symmetry of  $q^{\alpha\beta}$  and after the integration over  $x^\mu$  we have

$$\lim_{n\rightarrow 0} \frac{1}{n} G_1[q] = \int_{-\infty}^{\infty} Dy \log L(y), \quad (33)$$

where we used the abbreviation Eq. (28) and introduce

$$L(y) = 2\sqrt{\pi} \operatorname{Erfc}\left[\frac{\kappa + yq}{\sqrt{2(1-q^2)}}\right]. \quad (34)$$

The function  $L(y)$  is the main object that distinguishes the classical and the quantum perceptron. In the classical case we have

$$L(y) = 2\sqrt{\pi} \operatorname{Erfc}\left[\frac{\kappa + yq}{\sqrt{1-q}}\right]. \quad (35)$$

In the quantum case  $L(y)$  depends on  $q^2$ , since we are dealing with squared scalar products, which leads to an additional factor of two in the denominator of  $L(y)$ ; this factor will then be responsible for the increase of the storage capacity for the quantum case in comparison to the classical case.

##### C. Calculation of $G_2$ for spherical weights

We also assume replica symmetry of  $E^\alpha$  and  $F^{\alpha\beta}$  and perform the multi-dimensional Gaussian integral in Eq. (15) resulting in

$$G_2[E, F] = \log\left[(2\pi i)^{n/2}(\det M)^{-1/2}\right], \quad (36)$$

where we introduced the matrix

$$M^{ab} = (2E + F)\delta^{ab} - F. \quad (37)$$

The matrix  $M$  has  $n - 1$  degenerate eigenvalues  $\Lambda_1 = \dots = \Lambda_{n-1} = 2E + F$  and one non-degenerate eigenvalue  $\Lambda_n = 2E - (n - 1)F$  such that the determinant of the matrix  $M$  becomes

$$\log \det M = (n - 1) \log(2E + F) + \log[2E - (n - 1)F]. \quad (38)$$

#### D. Saddle-point equations of $G$ for spherical weights

Since  $G_1$  does not depend on  $E$  and  $F$  the saddle-point equations with respect to  $E$  and  $F$  are

$$0 = \frac{1}{n} \frac{\partial G}{\partial E} = -i + \frac{1}{n} \frac{\partial G_2}{\partial E}, \quad (39a)$$

$$0 = \frac{1}{n} \frac{\partial G}{\partial F} = \frac{i}{2}(n - 1)q + \frac{1}{n} \frac{\partial G_2}{\partial F}, \quad (39b)$$

with

$$\frac{1}{n} \frac{\partial G_2}{\partial E} = \frac{(n - 1)F + 2E(n - 2)}{2(2E + F)(-Fn + 2E + F)}, \quad (40a)$$

$$\frac{1}{n} \frac{\partial G_2}{\partial F} = \frac{(n - 1)F}{2(2E + F)(-Fn + 2E + F)}. \quad (40b)$$

Performing the limit  $n \rightarrow 0$  and solving for  $E$  and  $F$  results in

$$E = \frac{i(1 - 2q)}{2(1 - q)^2}, \quad (41a)$$

$$F = \frac{iq}{(1 - q)^2}. \quad (41b)$$

Further, we define the effective potential

$$g = \lim_{n \rightarrow 0} \frac{1}{n} G \quad (42)$$

and insert the solution of the saddle point equation into  $G$ . As a result, we obtain

$$g = \alpha \int_{-\infty}^{\infty} Dy \log L(y) + \frac{1}{2} \log(1 - q) + \frac{1}{2(1 - q)} \quad (43)$$

plus constant terms independent of  $q$ . We can interpret the logarithm of  $G$  as a free energy, which is a regular function of  $0 \leq q < 1$ , but has a singularity at  $q = 1$ . Employing the asymptotic expansion of  $\text{Erfc}(x) \approx \sqrt{\pi}x^{-1}e^{-x^2}\theta(x)$  for  $x \rightarrow \infty$ , we see that

$$g \simeq -\frac{\alpha}{2(1 - q)} \int_{-\infty}^{\infty} Dy(\kappa + y)^2 + \frac{1}{2(1 - q)}, \quad (44)$$

has two singular terms as  $q \rightarrow 1$ .

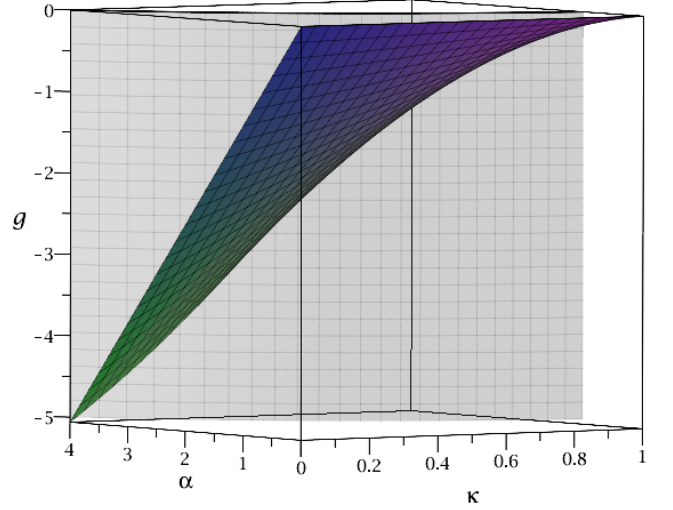


FIG. 4. **The effective potential for the spherical weights** We plot the effective potential  $g$  of Eq. (43). It changes from finite negative values below the  $\alpha_c$  curve to  $-\infty$  (represented by the grey area) above. The black line shows the  $\alpha_c$  curve given by Eq. (45).

If the second term dominates, it repulses the saddle point solution for  $q$  from being close to one. In this scenario, the order parameter  $q$  is finite as well as the function  $G$ . The relative volume shrinks in this regime exponentially with  $m$ . If the first term dominates above  $\alpha_c$ , the minimum of the free energy immediately shifts to  $q = 1$ , where  $g \rightarrow -\infty$ , so that the relative volume shrinks immediately to zero.

We plot the effective potential as a function of  $\alpha$  and  $\kappa$  in Fig. 4. This analysis implies that the critical value of the storage capacity is

$$\frac{\alpha_c}{2} \int_{-\kappa}^{\infty} Dy (\kappa + y)^2 = 1. \quad (45)$$

Performing the integral leads to the maximal critical storage capacity of  $\alpha_{c,\max} = 4$  for  $\kappa \rightarrow 0$ .

#### E. Calculation of $G_1$ for Gaussian distributed inputs

First, we define the matrix

$$A_{kk'} = \frac{1}{n} \sum_{\alpha} x^{\alpha} w_k^{\alpha} w_{k'}^{\alpha}, \quad (46)$$

which is spanned by the vectors  $w^{\alpha}$ . We can write its nontrivial eigenvectors as combinations of  $w^{\alpha}$ . The eigenvalue equation is

$$\frac{1}{n} \sum_{\alpha, k'} x^{\alpha} w_k^{\alpha} w_{k'}^{\alpha} \sum_{\beta} c_{\beta} w_{k'}^{\beta} = \Lambda \sum_{\alpha} c_{\alpha} w_k^{\alpha}. \quad (47)$$



All other eigenvectors of  $1 + 2i\hat{A}$  (orthogonal to the vectors  $w^\alpha$ ) are trivial – they correspond to eigenvalues 1 and do not contribute to the log det. Comparing coefficients, using the definition of  $q^{\alpha\beta}$  and assuming replica symmetry  $q^{\alpha\beta} = q$  for  $\alpha \neq \beta$ , leads to a closed equation

$$1 = \sum_a \frac{x^\alpha q}{\Lambda - x^\alpha (1 - q)} \quad (48)$$

for eigenvalues  $\Lambda$  of  $\hat{A}$ . Using the eigenvalues of  $\hat{A}$  we can rewrite  $G_1$  as

$$G_1[q] = \log \int \prod_\alpha d\lambda^\alpha \int \prod_\alpha dx^\alpha \frac{\exp(i \sum_\alpha x^\alpha \lambda^\alpha)}{\prod_n (1 + 2i\Lambda_n)}. \quad (49)$$

In order to rewrite the product of eigenvalues we transform the self-consistent equation for the eigenvalues  $\Lambda$  into the characteristic polynomial of  $\hat{A}$  to define the function

$$W(\Lambda, x) = \prod_\alpha [\Lambda - (1 - q)x^\alpha] - \sum_\alpha q x^\alpha \prod_{\alpha \neq \beta} [\Lambda - (1 - q)x^\beta]. \quad (50)$$

Next, we introduce the auxiliary quantity

$$L(\epsilon) = \log \det(1 + 2i\epsilon\hat{A}) = \sum_n \log(1 + 2i\epsilon\Lambda_n), \quad (51)$$

where we are interested in the value of  $L(1)$ . Differentiating with respect to  $\epsilon$  we obtain

$$\frac{dL}{d\epsilon} = \frac{n}{\epsilon} - \frac{1}{\epsilon} \sum_\Lambda \frac{1}{1 + 2i\Lambda\epsilon}. \quad (52)$$

The sum can be rewritten by using Cauchy's theorem and employing an appropriate contour  $\mathcal{C}$ . Using this integral representation for the sum we obtain

$$\frac{dL}{d\epsilon} = \frac{n}{\epsilon} + \frac{d}{d\epsilon} \log W(i/(2\epsilon), x). \quad (53)$$

Integrating  $\epsilon$  from 0 to 1 we get

$$L(1) = \log W(i/2, x) \quad (54)$$

since  $L(\epsilon)$  goes to zero for  $\epsilon \rightarrow 0$ . Expanding  $\Lambda$  in  $q$ , i.e., treating  $q$  as a perturbation,  $G_1$  becomes

$$G_1[q] = \log \int \prod_\alpha d\lambda^\alpha \int \prod_\alpha dx^\alpha \exp\left(i \sum_\alpha x^\alpha \lambda^\alpha\right) \times \frac{1}{\prod_\alpha \left(\frac{i}{2} - x_\alpha\right)} \left[1 + \sum_{\alpha, \beta} \frac{q^2 x^\alpha x^\beta}{\left(\frac{i}{2} - x_\alpha\right) \left(\frac{i}{2} - x_\beta\right)}\right]. \quad (55)$$

Performing the integration over  $x^\alpha$  and  $\lambda^\alpha$  gives

$$G_1(q) = \frac{\kappa n}{2} - \frac{1}{2} n q^2 (2 + \kappa)^2. \quad (56)$$

Due to the perturbative expansion in  $q$  the function  $G_1(q)$  does not exhibit any singularity at  $q = 1$  which will affect the nature of the phase transition.

## F. Saddle-point equations of $G$ for Gaussian distributed inputs

The effective potential of Eq. (13) becomes

$$g = \alpha \left[ \frac{\kappa}{2} - \frac{1}{2} q^2 (2 + \kappa)^2 \right] + \frac{1}{2} \log(1 - q) + \frac{1}{2(1 - q)}, \quad (57)$$

plus constant terms independent of  $q$ . This function does contain a singular term  $(1 - q)^{-1}$ , which repulses the saddle point solutions for the minimal value away from  $q = 1$ . Indeed, taking the derivative of  $G$  with respect to  $q$  gives

$$\alpha(2 + \kappa)^2 q = \frac{q}{2(1 - q)^2}. \quad (58)$$

This equation has a trivial solution  $q = 0$  for which

$$g = (\alpha\kappa)/2, \quad (59)$$

and a non-trivial solution, which exists for  $2\alpha(2 + \kappa)^2 \geq 1$ . The critical value of the storage capacity is given by (see App. D)

$$\alpha_c = \frac{1}{2(2 + \kappa)^2}. \quad (60)$$

Note that the phase transition in this case has a different character: for both solutions  $g$  takes a finite value, but it changes from  $(\alpha\kappa)/2$  in the "easy to learn" phase to a larger values in the "hard to learn phase", see Fig. 5. This behavior might be the result of expansion in  $q$  that we used to obtain the effective potential. Further, the effective potential might be the first term of expansion of  $(1 - q^2)^{-1}$  and we discuss this idea in App. D, which will bring us back to the volume shrinking phase transition à la Gardner.

## G. Calculation of $G_2$ for Ising weights

Assuming replica symmetry of  $F^{ab}$  and averaging over the binary weights, Eq. (24) becomes

$$G_2 = -\frac{1}{2} F n + n \int_{-\infty}^{\infty} Dz \log \left[ 2 \cosh(z\sqrt{F}) \right], \quad (61)$$

as in the classical case [54].

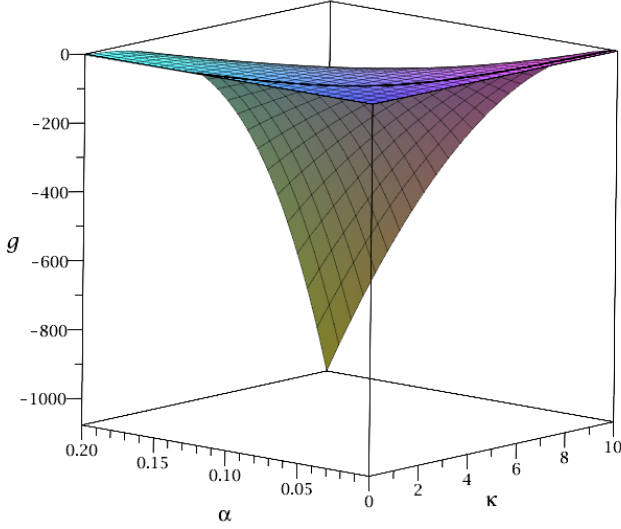


FIG. 5. **The effective potential of Gaussian distributed inputs** We plot the effective potential  $g$ . It changes from small values close to zero of Eq. (59) below the  $\alpha_c$  curve to larger negative values of Eq. (57) above. The black line shows the  $\alpha_c$  curve given by Eq. (60).

#### H. Saddle-point equations of $G$ for Ising weights

The effective potential with replica symmetry of  $q^{ab}$  and  $F^{ab}$  becomes

$$g = \alpha \int_{-\infty}^{\infty} Dy \log L(y) + R(F, q) \quad (62)$$

with

$$R(F, q) = -\frac{1}{2}F(1-q) + \int_{-\infty}^{\infty} Dz \log \left[ 2 \cosh \left( z\sqrt{F} \right) \right]. \quad (63)$$

Then, the saddle-point equation with respect to  $F$  is

$$-\frac{1}{2}(1-q) + \int_{-\infty}^{\infty} Dz \frac{z}{2\sqrt{F}} \tanh \left( z\sqrt{F} \right) = 0, \quad (64)$$

which is similar to equation obtained for the classical perceptron with binary weights [37], where it was argued that the solution with  $F \rightarrow \infty$  as  $q \rightarrow 1$  is invalid. Instead, for the correct solution of the classical perceptron problem, replica-symmetry breaking must be taken into account.

Here, we analyze results for replica symmetric case and compare them with Monte Carlo simulations. For the quantum perceptron,  $F$  is a well defined function of  $q$ , and it tends to infinity as  $q \rightarrow 1$ . The last equation can be solved

$$\sqrt{F} \approx \sqrt{\frac{2}{\pi}} \frac{1}{(1-q)}, \quad (65)$$

where  $\text{sign}(x) = x/|x|$  and we approximated the  $\tanh$  by  $\text{sign}(x)$ .

Comparing the leading terms when  $q \rightarrow 1$ , we arrive at

$$g \approx \frac{1}{(1-q)} \left[ -\frac{\alpha}{4} \int_{-\kappa}^{\infty} Dy (\kappa + y)^2 + \frac{1}{\pi} \right]. \quad (66)$$

In this way we obtain the critical value

$$\alpha_c(\kappa) = \frac{4}{\pi} \left[ \int_{-\kappa}^{\infty} Dy (\kappa + y)^2 \right]^{-1}, \quad (67)$$

which implies the maximal value of  $\alpha_c(0) = 8/\pi$ . In contrast the MC simulations suggest that  $\alpha_c(0) \simeq 0$  as illustrated in Fig. 3. As in the classical case, we interpret this discrepancy as the necessity of replica symmetry breaking.

## V. ACKNOWLEDGMENTS

ICFO group acknowledges support from: ERC AdG NOQIA; Agencia Estatal de Investigación (R&D project CEX2019-000910-S, funded by MCI/AEI/10.13039/501100011033, Plan National FIDEUA PID2019-106901GB-I00, FPI, QUANTERA MAQS PCI2019-111828-2, QUANTERA DYNAMITE PCI2022-132919, Proyectos de I+D+I “Retos Colaboración” QUSPIN RTC2019-007196-7), MCIN via European Union NextGenerationEU (PRTR); Fundació Cellex; Fundació Mir-Puig; Generalitat de Catalunya through the European Social Fund FEDER and CERCA program (AGAUR Grant No. 2017 SGR 134, QuantumCAT U16-011424, co-funded by ERDF Operational Program of Catalonia 2014-2020); EU Horizon 2020 FET-OPEN OPTologic (Grant No 899794); National Science Centre, Poland (Symfonia Grant No. 2016/20/W/ST4/00314); European Union’s Horizon 2020 research and innovation programme under the Marie-Sklódowska-Curie grant agreement No 101029393 (STREDCH) and No 847648 (“La Caixa” Junior Leaders fellowships ID100010434: LCF/BQ/PI19/11690013, LCF/BQ/PI20/11760031, LCF/BQ/PR20/11770012, LCF/BQ/PR21/11840013); European Union’s Horizon 2020 research and innovation programme under the Marie Skłodowska-Curie grant agreement No 847517.

## VI. DATA AVAILABILITY

The data that support the findings of this study are available from the corresponding author upon request.

## VII. AUTHOR CONTRIBUTIONS

All authors contributed to the design and implementation of the research, to the analysis of the results and to the writing of the manuscript. The Authors declare no

Competing Financial or Non-Financial Interests. Correspondence and requests for materials should be addressed to A.G. (gratsea.katerina@gmail.com).

### Appendix A: Details on the quantum perceptron proposed in [40]

The first unitary  $U_{\vec{i}}$  should fulfill

$$|\psi_{\vec{i}}\rangle = U_{\vec{i}}|0\rangle^{\otimes N}, \quad (\text{A1})$$

and in this way encodes the information on  $N$  qubits. Particularly, any  $m \times m$  unitary matrix with the first column being identical with  $\vec{i}$  and normalized is a valid candidate for such a unitary. The information is processed by applying the second unitary  $V_{\vec{w}}$  which fulfills

$$V_{\vec{w}}|\psi_{\vec{w}}\rangle = |1\rangle^{\otimes N} = |m-1\rangle. \quad (\text{A2})$$

Applying the unitary  $V_{\vec{w}}$  on the encoded state leads to

$$|\phi_{\vec{i},\vec{w}}\rangle \equiv V_{\vec{w}}|\psi_{\vec{i}}\rangle = \sum_{j=0}^{m-1} c_j |j\rangle. \quad (\text{A3})$$

Performing multi-controlled NOT gates with a readout qubit leads to the state

$$|\phi_{i,w}\rangle |0\rangle = \sum_{j=0}^{m-2} c_j |j\rangle |0\rangle + c_{m-1} |m-1\rangle |1\rangle. \quad (\text{A4})$$

As a result, when measuring 1 on the readout qubit, the probability amplitude is

$$|c_{m-1}|^2 = |\vec{i}^\mu \cdot \vec{w}|^2. \quad (\text{A5})$$

### Appendix B: Abbreviations

In this appendix, we summarize the abbreviation used in the main text. In Eq. (5) and Eq. (6) we used

$$\int_w = \int_{-\infty}^{\infty} \prod_k dw_k, \quad (\text{B1})$$

and in Eq. (9) the measure is

$$\begin{aligned} \int_w \int_\lambda \int_x \int_E &= \int_{-\infty}^{\infty} \prod_k dw_k \int_{\kappa}^{\infty} \prod_{\mu} d\lambda^\mu \\ &\times \int_{-\infty}^{\infty} \prod_{\mu} \frac{dx^\mu}{2\pi} \int_{-\infty}^{\infty} \frac{dE}{2\pi}, \end{aligned} \quad (\text{B2})$$

in Eq. (12) the abbreviation means

$$\int_F \int_q \int_E = \int_{-\infty}^{\infty} \prod_{\alpha < \beta} dq^{\alpha\beta} \int_{-\infty}^{\infty} \prod_{\alpha < \beta} \frac{dF^{\alpha\beta}}{2\pi} \int_{-\infty}^{\infty} \prod_{\alpha} \frac{dE^{\alpha}}{2\pi}, \quad (\text{B3})$$

and in Eq. (30) we used

$$\begin{aligned} \int_w \int_\lambda \int_x \int_E \int_q \int_F &= \int_{-\infty}^{\infty} \prod_{k,\alpha} dw_k^\alpha \int_{\kappa}^{\infty} \prod_{\mu,\alpha} d\lambda_\mu^\alpha \int_{-\infty}^{\infty} \prod_{\alpha,\mu} \frac{dx_\mu^\alpha}{2\pi} \\ &\times \int_{-\infty}^{\infty} \prod_{\alpha} \frac{dE^\alpha}{2\pi} \int_{-\infty}^{\infty} \prod_{\alpha < \beta} dq^{\alpha\beta} \int_{-\infty}^{\infty} \prod_{\alpha < \beta} \frac{dF^{\alpha\beta}}{2\pi}. \end{aligned} \quad (\text{B4})$$

### Appendix C: Monte Carlo simulation

We apply the Monte Carlo simulation of the classical perceptron with Ising weights [55] to the quantum perceptron. Here, we elaborate the details of the Monte Carlo simulation.

The first pattern  $i_j^1 = \pm 1$  is chosen at random and we fix a certain threshold  $\kappa$ . Then, we go through all possible realizations of the weights and keep only the weights that satisfy the given threshold  $\kappa$ . This forms the remaining set of the weights. Then, a second pattern is chosen at random and we go through all possible realizations of the remaining set of the weights to keep again only the subset of weights which satisfy the given threshold  $\kappa$ . Then, we continue by choosing more random patterns and updating the set of the weights that fulfill the given threshold. After a certain number of  $P$  patterns that have been introduced to the perceptron, no choice for the weights exist for  $P+1$  patterns. This means that for this sample the system can store exactly  $P$  patterns.

Therefore, the value of  $P$  depends on the random choices of the  $\sum i_j^\mu = \pm 1$  and the threshold  $\kappa$ . The threshold  $\kappa$  in the classical case is zero, since the output is either  $\pm 1$ . For the quantum case, the threshold  $\kappa$  is  $m/2$  since  $\kappa \in [0, m]$ . We need to average  $P$  over many samples and define the estimate of the storage capacity for a system of size  $N_s$

$$\alpha(N_s) = \frac{\langle P \rangle}{N_s}. \quad (\text{C1})$$

For the numerical simulations in Fig. 3,  $N_s$  is equal to  $N$  and  $m$  for the classical and quantum perceptron, respectively. Moreover, we have  $2^N$  and  $2^m$  realizations of the weights for the classical and quantum models, respectively. We used 10000 samples for each simulation and we performed them three times to estimate the error. In Fig. 3, we choose odd values of  $N$  to always have  $\pm 1$  for the output and we use  $m = 8, 16, 32$  since for larger  $m$  the computation becomes intractable.

### Appendix D: Speculations about the Gaussian inputs

In the derivation of the basic expression

$$g = \alpha \left[ \frac{\kappa}{2} - \frac{1}{2} q^2 (2 + \kappa)^2 \right] + \frac{1}{2} \log(1 - q) + \frac{1}{2(1 - q)}, \quad (\text{D1})$$

where we used an expansion in  $q$  to study the  $q \rightarrow 1$  behaviour. The next order contribution in the effective potential is presumably

$$\left[ \frac{\kappa}{2} - \frac{1}{2} q^2 (2 + \kappa)^2 \right] \approx \left[ \frac{\kappa}{2} + \frac{1}{2} (2 + \kappa)^2 - \frac{1}{2(1 - q^2)} (2 + \kappa)^2 \right] \text{ implying maximal } \alpha_c(\kappa = 0) = 1/8.$$

and suggests that

$$\alpha_c(2 + \kappa)^2/2 = 1,$$

- 
- [1] M. van Gerven and S. Bohte, *Frontiers in computational neuroscience* **11**, 114 (2017).
  - [2] G. Carleo, I. Cirac, K. Cranmer, L. Daudet, M. Schuld, N. Tishby, L. Vogt-Maranto, and L. Zdeborová, *Reviews of Modern Physics* **91**, 045002 (2019).
  - [3] S. Angra and S. Ahuja, in *2017 International Conference on Big Data Analytics and Computational Intelligence (ICBDAC)* (2017) pp. 57–60.
  - [4] J. Schmidhuber, *Neural Networks* **61**, 85 (2015).
  - [5] F. Rosenblatt, *Psychological Review* **65**, 386 (1958).
  - [6] M. Minsky and S. Papert, *Perceptrons: An Introduction to Computational Geometry* (MIT Press, Cambridge, MA, USA, 1969).
  - [7] J. VanderPlas, A. J. Connolly, Z. Ivezic, and A. Gray, in *2012 Conference on Intelligent Data Understanding* (2012) pp. 47–54.
  - [8] A. N. Michel and J. A. Farrell, *IEEE Control Systems Magazine* **10**, 6 (1990).
  - [9] E. Ikonomakis, S. Kotsiantis, and V. Tampakas, *WSEAS transactions on computers* **4**, 966 (2005).
  - [10] J. Zhu, T. Zhang, Y. Yang, and R. Huang, *Applied Physics Reviews* **7**, 011312 (2020).
  - [11] J. Biamonte, P. Wittek, N. Pancotti, P. Rebentrost, N. Wiebe, and S. Lloyd, *Nature* **549**, 195 (2017).
  - [12] M. Schuld, I. Sinayskiy, and F. Petruccione, *Physics Letters A* **379**, 660 (2015).
  - [13] M. Schuld, I. Sinayskiy, and F. Petruccione, *Quantum Information Processing* **13**, 2567 (2014).
  - [14] B. Müller, J. Reinhardt, and M. T. Strickland, *Neural Networks*, Physics of Neural Networks (Springer Berlin Heidelberg, Berlin, Heidelberg, 1995).
  - [15] M. Shcherbina and B. Tirozzi, *Communications in Mathematical Physics* **234**, 383 (2001).
  - [16] A. Gratsea and P. Huembeli, “The effect of the processing and measurement operators on the expressive power of quantum models,” (2022).
  - [17] V. Dunjko and H. J. Briegel, *Reports on Progress in Physics* **81**, 074001 (2018).
  - [18] G. Carleo and M. Troyer, *Science* **355**, 602 (2017).
  - [19] P. Wittek, *Quantum Machine Learning* (Elsevier Science & Technology, San Diego, 2014).
  - [20] N. Kåring, A. Dawid, K. Kottmann, M. Lewenstein, K. Sengstock, A. Dauphin, and C. Weitenberg, *Machine Learning: Science and Technology* **2**, 035037 (2021).
  - [21] H.-Y. Huang, M. Broughton, M. Mohseni, R. Babbush, S. Boixo, H. Neven, and J. R. McClean, “Power of data in quantum machine learning,” (2021), [arXiv:2011.01938](https://arxiv.org/abs/2011.01938).
  - [22] J. Preskill, *Quantum* **2**, 79 (2018).
  - [23] M. Schuld and N. Killoran, *Phys. Rev. X Quantum* **3**, 030101 (2022).
  - [24] M. S. Rudolph, J. Miller, J. Chen, A. Acharya, and A. Perdomo-Ortiz, “Synergy between quantum circuits and tensor networks: Short-cutting the race to practical quantum advantage,” (2022).
  - [25] J. Hopfield, *Proc. Nat. Acad. Sci.* **79**, 2554 (1982).
  - [26] D. Amit, *Modelling Brain Function* (Cambridge University Press, 1989).
  - [27] A. Decelle and C. Furtlehner, *Phys. Rev. Lett.* **127**, 158303 (2021).
  - [28] A. Pozas-Kerstjens, G. Muñoz-Gil, M. Ángel García-March, A. Acín, M. Lewenstein, and P. R. Grzybowski, *Mach. Learn.: Sci. Techn.* **2**, 025026 (2021).
  - [29] N. Tishby,.
  - [30] D. E. Rumelhart, J. L. McClelland, and PDP Research Group, eds., *Parallel Distributed Processing. Volume 1: Foundations* (MIT Press, Cambridge, MA, 1986).
  - [31] J. L. McClelland, D. E. Rumelhart, and PDP Research Group, eds., *Parallel Distributed Processing. Volume 2: Psychological and Biological Models* (MIT Press, Cambridge, MA, 1986).
  - [32] J. Fraxanet, T. Salamon, and M. Lewenstein, *Lecture Notes in Physics*, **1000**, [arXiv:2204.08905](https://arxiv.org/abs/2204.08905).
  - [33] H. Nishimori, *Statistical Physics of Spin Glasses and Information Processing* (Oxford University Press, 2001).
  - [34] B. Aubin, W. Perkins, and L. Zdeborová, *Journal of Physics A: Mathematical and Theoretical* **52**, 294003 (2019).
  - [35] N. Davey and R. Adams, *Connection Science* **16**, 47 (2004).
  - [36] E. Gardner, *Journal of Physics A: Mathematical and General* **21**, 257 (1988).
  - [37] E. Gardner and B. Derrida, *Journal of Physics A: Mathematical and General* **21**, 271 (1988).
  - [38] H. Sompolinsky, in *Heidelberg Colloquium on Glassy Dynamics*, edited by J. L. van Hemmen and I. Morgenstern (Springer Berlin Heidelberg, Berlin, Heidelberg, 1987) pp. 485–527.
  - [39] J. Ding and N. Sun, in *Proceedings of the 51st Annual ACM SIGACT Symposium on Theory of Computing* (ACM, New York, NY, USA, 2019) pp. 816–827.
  - [40] F. Tacchino, C. Macchiavello, D. Gerace, and D. Bajoni, *npj Quantum Information* **5**, 26 (2019).
  - [41] M. Lewenstein, *Journal of Modern Optics* **41**, 2491 (1994), <https://doi.org/10.1080/09500349414552331>.
  - [42] K. Życzkowski, P. Horodecki, A. Sanpera, and M. Lewenstein, *Phys. Rev. A* **58**, 883 (1998).
  - [43] M. Lewenstein, A. Gratsea, A. Riera-Campenay, A. Aloy, V. Kasper, and A. Sanpera, *Quantum Science and Technology* **6**, 045002 (2021).
  - [44] M. G. Díaz, G. Sentís, R. Muñoz-Tapia, and A. Sanpera, (2021).
  - [45] E. Torrontegui and J. J. García-Ripoll, *Europhysics Letters* **125**, 30004 (2019).
  - [46] K. Beer, D. Bondarenko, T. Farrelly, T. J. Osborne, R. Salzmann, D. Scheiermann, and R. Wolf, *Nature Communications* **11** (2020), [10.1038/s41467-020-14454-2](https://doi.org/10.1038/s41467-020-14454-2).

- [47] D. Sherrington and S. Kirkpatrick, *Physical Review Letters* **35**, 1792 (1975).
- [48] M. Mezard, G. Parisi, and M. Virasoro, *Spin Glass Theory and Beyond* (WORLD SCIENTIFIC, 1986).
- [49] M. Andrecut and M. K. Ali, *International Journal of Modern Physics B* **17**, 2447 (2003).
- [50] D. Ventura and T. Martinez, *Information Sciences* **124**, 273 (2000).
- [51] L. G. Wright and P. L. McMahon, in *Conference on Lasers and Electro-Optics* (OSA, Washington, D.C., 2020) p. JM4G.5.
- [52] F. Benatti, G. Gramegna, and S. Mancini, *Journal of Physics A: Mathematical and Theoretical* (2022).
- [53] J. F. Fontanari and R. Meir, *Journal of Physics A* **22** (1989).
- [54] W. Krauth and M. Mézard, *Journal de Physique* **50**, 3057 (1989).
- [55] E. Gardner and B. Derrida, *Journal of Physics A: Mathematical and General* **22**, 1983 (1989).
- [56] M. Schuld, I. Sinayskiy, and F. Petruccione, *Physics Letters A* **379**, 660 (2015).
- [57] A. Gratsea and P. Huembeli, “Exploring quantum perceptron and quantum neural network structures with a teacher-student scheme,” (2021).
- [58] V. Kasper, D. González-Cuadra, A. Hegde, A. Xia, A. Dauphin, F. Huber, E. Tiemann, M. Lewenstein, F. Jendrzejewski, and P. Hauke, “Universal quantum computation and quantum error correction with ultracold atomic mixtures,” (2020), [arXiv:2010.15923 \[cond-mat.quant-gas\]](#).
- [59] J. R. Weggemans, A. Urech, A. Rausch, R. Spreuw, R. Boucherie, F. Schreck, K. Schoutens, J. Minář, and F. Speelman, “Solving correlation clustering with qaoa and a rydberg qudit system: a full-stack approach,” (2021), [arXiv:2106.11672 \[quant-ph\]](#).
- [60] M. Ringbauer, M. Meth, L. Postler, R. Stricker, R. Blatt, P. Schindler, and T. Monz, “A universal qudit quantum processor with trapped ions,” (2021), [arXiv:2109.06903 \[quant-ph\]](#).
- [61] G. Kohring, *Journal de Physique* **51**, 145 (1990).